Anti-infiltration for Fabrication of a Suspended Nanoparticle Layer on Porous Close-Packed Colloidal Arrays

Lay K. Teh,* Qingfeng Yan,† and Chee C. Wong

School of Materials Science and Engineering, Nanyang Technological University, N4.1-B3-02, 50 Nanyang Avenue, Singapore 639798, Singapore, and Department of Chemistry, Tsinghua University, Room 403, Beijing 100084, China

ABSTRACT We develop a new method to fabricate suspended sheets of nanocrystals (NCs) on porous surfaces. The method relies on the resistance of an aqueous suspension droplet to infiltrate a porous network; hence, the method is named anti-infiltration. The process works by combining fluid dynamics of a liquid droplet during impact/absorption onto a porous surface with the convective self-assembly of NCs. The immobilization of the liquid droplet edge due to the self-assembly of NCs at the meniscus is harnessed to halt the lateral spreading of the droplet and, consequently, the capillary penetration of the liquid immediately after droplet impact. Further capillary penetration of the liquid is drastically reduced because of the competition between capillary forces and convective losses as well as the rapid occlusion of the pores as soon as a continuous NC film has formed upon evaporation of the suspension. This method holds promise for a wide variety of optoelectronic, sensing, and separation membrane applications. As an example, we demonstrate that these suspended NC layers are suitable candidates as planar defects embedded within a colloidal photonic crystal.

KEYWORDS: self-assembly • suspended films • porous media • nanoparticles • liquid droplets

INTRODUCTION

Suspended thin films covering patterned/porous surfaces have received substantial interest for photonic (1), sensing (2), and separation membrane (3) applications, with considerable efforts on ultrathin suspended sheets. For example, a lithographical approach has been used to create silicon-, ceramic-, or carbon-based free-standing membranes (4−6), as well as defects embedded within periodic photonic nanostructures (7). While lithography is a well-established fabrication technique for obtaining intricate microstructures, it involves complicated procedures and reducing the lateral dimensions for high-resolution sensing membranes drastically compromises their flexural compliance. In contrast, a variety of wet processes are able to produce free-standing films readily (2, 8−14). In these cases, the transfer of the films to the desired porous substrates is necessary. Recently, free-standing inorganic films covering an array of holes have been obtained with the use of sacrificial surfactant bilayers (15). Others have also used sacrificial filling in the deposition of defect layers onto a porous opal surface for photonic applications (16). The need for the sacrificial material highlights the challenging problem of growing suspended layers on top of porous structures.

Here we borrow a trick from the fluid motion in porous media and offer an alternative approach to forming suspended layers of self-assembled nanocrystals (NCs) on porous surfaces. Our "anti-infiltration" approach offers an edge over standard techniques because it involves simple solution-based deposition processes. Porous opals with regular close-packed sphere arrays were used as the porous substrates. By simple deposition of a sessile drop of nanocolloids of controlled volume onto the opal surface and fine-tuning of the evaporation of the solvent, a free-standing film of NCs could be readily obtained through self-assembly of the NCs at the water−opal interface, without penetrating into the opal voids below. We also demonstrate the use of this technique to introduce a defect slab into opaline photonic crystals. This enables the localization of defect states within a photonic band gap (17), an optical analogy of doping in semiconductors.

RESULTS AND DISCUSSION

Rationale of the Method. We first discuss the critical conditions for the wetting of porous surfaces. The idea is rooted in the kinetic energy considerations of a liquid droplet impinging on a porous surface (18, 19). The evolution of the shape of the droplet is governed by three main mechanisms: (i) initial momentum of the droplet, (ii) resistance imposed by the porous substrate, which tends to hinder liquid penetration into the substrate, and (iii) capillary force to draw the liquid into the substrate. This can be described in two stages, as shown in Figure 1a. When a droplet of initial radius R_0 settles on a porous medium, there is an immediate enlargement of the droplet size to R_e to dissipate the impact momentum (stage I droplet impact). Subsequently, the droplet is further enlarged to R_c to dissipate the impact momentum completely by capillary spreading upon the surface coupled with sorption into the pores (stage II spread-

* Corresponding author. E-mail: laykuan@pmail.ntu.edu.sg.
Received for review November 22, 2008 and accepted February 23, 2009
† Tsinghua University.
DOI: 10.1021/am800188z

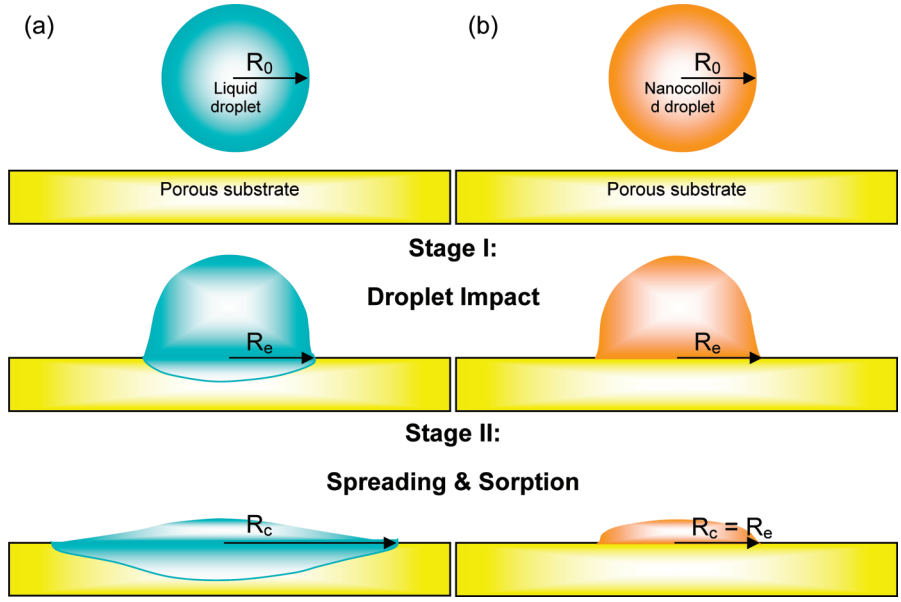

FIGURE 1. Evolution of the shape of a droplet of (a) pure liquid and (b) colloidal suspension striking on a porous surface. R_0 is the initial radius of the droplet, R_e is the radius of the droplet immediately after impact, and R_c is the final radius of the droplet when the kinetic energy is completely consumed. In general, $R_0 < R_e < R_c$. $R_e = R_c$ in the case of droplet immobilization with zero capillary spreading and sorption.

ing and sorption) at a certain spread ratio. The liquid penetration slows down gradually as the droplet radius increases, for reasons of the conservation of mass and momentum. The magnitude of the fluid velocity is a balance between momentum dissipation due to viscous drag of the porous substrate and capillary penetration (18). In some cases, when the resistance of the substrate is large enough to rapidly reduce the initial droplet momentum, the droplet is prevented from penetrating into the substrate and is thus suspended as a liquid film on top of the porous surface at stage I. This is dependent largely on fluid-flow parameters such as the Reynolds number (*Re*) and Darcy number (*Da*), which indicate respectively the strength and rate of the momentum dissipation by viscous drag of the solid matrix of the substrate. At stage II, *Re* determines the degree of lateral spreading and liquid penetration, while the liquid continues to spread laterally as it would on a solid flat surface for extremely small *Da*. We postulate that when the viscous drag is sufficiently strong to dissipate most of the initial droplet momentum, the droplet is immobilized, limiting the lateral spreading on top of the porous surface such that the droplet size remains as R_e at stage II with negligible capillary penetration and sorption inside the substrate (see Figure 1b for an example). This forms the basis for anti-infiltration. Besides droplet impingement and spreading, another crucial aspect of the anti-infiltration method relies on the self-organizational ability of the NCs in suspension.

The self-organization of highly uniform NCs has been extensively studied recently (20). NC superlattices can be obtained by gentle evaporation of the NC dispersion. It was found that 3D-faceted colloidal crystals are formed in the bulk of the solution by homogeneous nucleation driven by interparticle interactions. A thin, ordered superlattice of dots can be produced by heterogeneous nucleation at a solid or liquid interface, which acts as a template for providing dimensional restriction (21). Recently, free-floating nanocrystallite sheets of a monolayer and bilayers have also been generated in solution with the combination of anisotropic electrostatic interaction and directional hydrophobic attraction (22).

We have used commercial nanocolloids of CdSe/ZnS core–shell NCs (from Evident Technologies) stabilized in water. The crystal diameter (*d*) of the NCs used was 3.2 nm (the approximate hydrodynamic diameter is 25 nm). In all experiments, a 30 μL droplet of the NC suspension was deposited gently on a SiO_2–opal. The surface of a typical porous opal formed by convective self-assembly of submicron colloidal spheres is shown in Figure 2a [high-resolution transmission electron microscopy (TEM) images and an optical spectrum of the NC film are given in Figures S1 and S2 in the Supporting Information]. By simple geometry, the diameter of the largest sphere that could pass through the interstices between three touching spheres in the close-packed plane corresponds to $d = 0.155D$; in our case, $d \approx 43$ nm. Figure 2b shows the cross section of a suspended layer of NCs on a SiO_2–opal made of 300 nm spheres deposited at 55 °C. The as-deposited nanocrystallite layer has sufficient structural continuity to float off as a sheet onto a liquid surface when the sample was placed vertically into a vial of water. Despite the hydrophilicity of the SiO_2–opal and the minute NC size, there is no sign of NCs infiltrating into the porous opal voids. This implies that the resistance to penetration is strong enough to rapidly reduce most of the initial droplet momentum, such that the nanocolloid droplet lies suspended as a NC sheet on top of the SiO_2–opal after complete drying (see Figure 1b). However, a small enough *Da* for zero capillary penetration and sorption into the SiO_2–opal of submicron spheres has not been attained based on the droplet configuration in our experiments.

Anti-infiltration Mechanism. We attribute the strong resistance to fluid penetration to be a consequence of

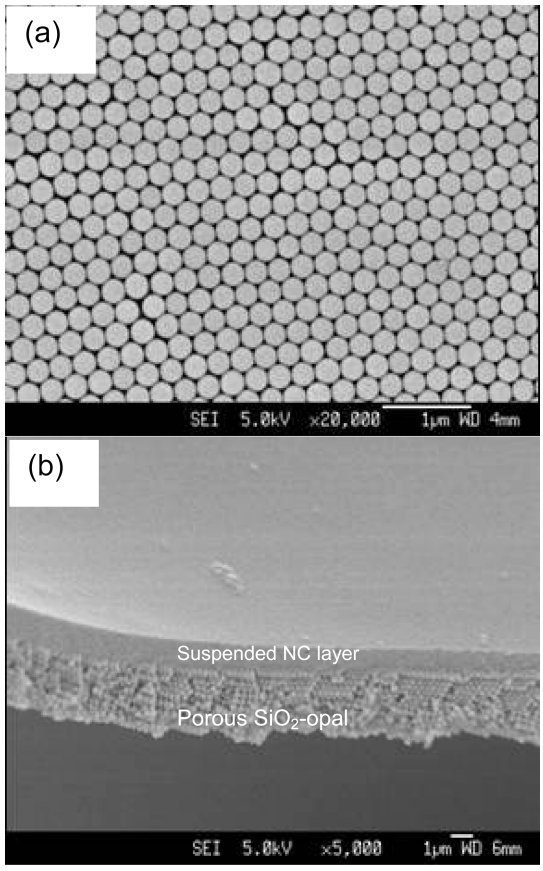

FIGURE 2. (a) Top view of a typical porous opal consisting of close-packed sphere arrays. (b) Suspended layer of NCs on a 300 nm SiO_2−opal.

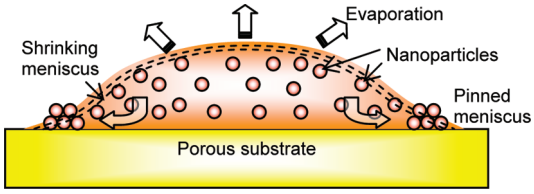

FIGURE 3. Schematic of the evaporation process of the nanocolloid droplet.

meniscus pinning of the nanocolloid droplet along its perimeter during drying of the nanocolloid. This is the well-known static nature of the contact line of a drop of colloidal suspension accompanied with a decreasing contact angle during drying, in contrast to the moving contact line of a pure liquid to reach the equilibrium contact angle. As shown in Figure 3, the solvent loss (highest evaporation rate at the drop edge) leads to convective mass transport of NCs to the meniscus of the droplet where self-assembly takes place, driven by the natural interaction forces in charge-stabilized colloids and the capillary forces built into the equilibrium shape of the sessile drop (23−25). As such, the capillary forces for spreading, had the fluid been a pure liquid, now serve as the driving force for the self-assembly of colloids and counteract the capillary sorption into the substrate. Consequently, the NCs accumulate and induce viscous drag to dissipate most of the initial droplet momentum. This immobilizes the nanocolloid droplet and limits the lateral spreading as well as infiltration into the substrate.

While the growth continues with meniscus deformation at the droplet edge on top of the substrate, nanocolloid in the middle of the droplet infiltrates into the substrate because of the radial projection of liquid, albeit at a much slower rate (the fluid flow inside the porous substrate is reduced by as much as 2 orders of magnitude in terms of the unit velocity (18)). Our observations reveal that a water droplet penetrates into the substrate considerably faster than a nanocolloid droplet. This is consistent with the numerical results obtained in ref 18, whereby the complete sorption into the substrate for a system with viscous effects strong enough to halt the lateral spreading is nearly 1000 times slower than a system with small viscous effects, in which the liquid spreads and absorbs freely. In this work, capillary penetration and sorption are also constantly competing with the rapid solvent loss by evaporation at raised temperatures throughout the process. As the droplet evaporates and the meniscus shrinks, it leaves behind a typical ring pattern (24, 26, 27) consisting of self-assembled NCs on the opal surface (see Figures S3−S5 in the Supporting Information for details of the ring pattern). The size of the NC layers is larger than the interstices, preventing further infiltration into the pores. This generates a filter cake, which serves to impede the infiltration.

To verify the immobilization of the nanocolloid droplet to hinder capillary spreading and sorption, we repeated the same experiment with a sessile drop of water. The diameter of the water droplet was found to be larger than that of the nanocolloid droplet (∼12 vs ∼8 mm). This is believed to be a result of the lateral capillary spreading and sorption that has occurred in the case of the water droplet due to the absence of meniscus pinning.

Following the concept of the effective density of assembled particles introduced in a previous report (28), the effective density of the assembled NCs is $(\pi/3\sqrt{3})\rho_{NCs} \sim 0.6$ (the specific gravity of the NCs is ∼1.0), which is lower than the density of water. Hence, it is reasonable to assume that the assembled NCs will float on the water surface as observed experimentally.

Anti-infiltration for the Introduction of Planar Defects in Colloidal Photonic Crystals. Figure 4a shows the fabrication scheme for inserting a defect slab into opaline photonic crystals by sequentially stacking opals (29) and NC sheets deposited by convective self-assembly and anti-infiltration. The final structure with a NC planar defect is shown in Figure 4b. The scanning electron micrographs in Figure 4c,d show a closeup of the NC−opal interface for opals made of two different materials: SiO_2 (hydrophilic) and polystyrene (hydrophobic). For NCs deposited on SiO_2−opal, the nanocrystallite layer follows the contour of the bottom opal, and thus the bottom surface of the defect layer appears undulated. In contrast, the self-assembled layer of NCs lies flat on top of the polystyrene−opal. This suggests that the polystyrene−opal surface is sufficiently hydrophobic that aqueous nanocolloid tends to bridge the highest points of the spheres, suspending across the surface of the undulating bottom opal.

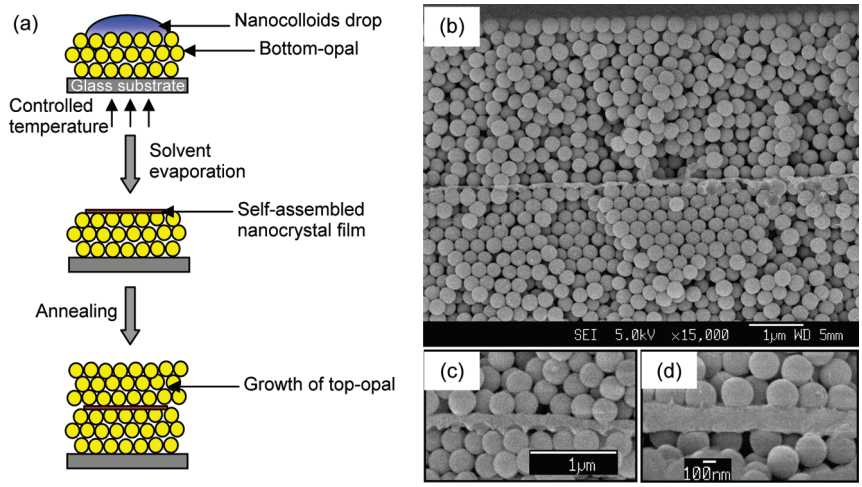

FIGURE 4. (a) Schematic illustration of the introduction of nanocrystalline planar defects into opaline colloidal crystals. (b) Cross section of a SiO_2–opal with an embedded planar defect composed of NCs. Self-assembly of nanocolloids on bottom opals with different wettability: (c) hydrophilic SiO_2–opal; (d) hydrophobic polystyrene–opal. Anti-infiltration prevents the penetration of NCs into the bottom opal, evident by the distinct NC–opal interface.

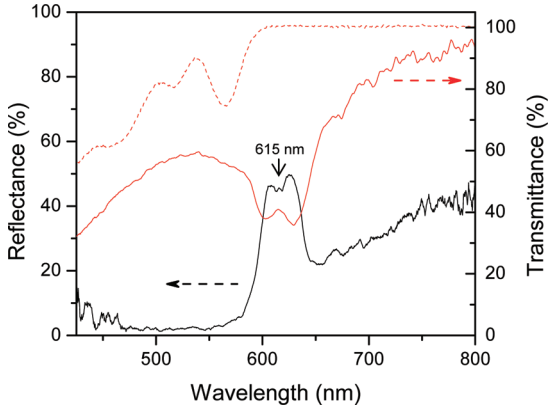

FIGURE 5. Optical reflection and transmission spectra of a SiO_2–opal embedded with a NC planar defect. The arrow indicates the peak and dip position. The dashed line shows the absorption edge of the NC at ~560 nm.

To confirm light modulation by the introduction of the NC defect layer, we examined the optical characteristics of the opaline PhCs with a NC planar defect. The reflectance spectrum in Figure 5 shows a dip within the spectral range of the photonic pseudogap of the defect-free opal. The dip corresponds to a defect state at which transmission is allowed, which is coupled through the planar defect. The corresponding transmission spectrum is also included to provide complementary evidence for the presence of a planar defect, showing that a peak appears at almost the same position (615 nm) as the transmission dip.

CONCLUSIONS

We have developed an anti-infiltration method derived from the dynamic balance between capillary penetration and convective self-assembly of nanoparticles to form suspended NC layers on porous opal surfaces. Our method, based on a sessile drop configuration, is simple and fast, although the thickness control is not yet perfect. It can cover an array of pores in a one-step process without the need of removing sacrificial sublayers. It is applicable for substrates with different pore shapes, sizes, and arrangements. This approach is extendable to any uniform nanocolloids and opens up the opportunity for a wide variety of new functionalities derived from the collective properties of self-assembled NCs. The potential of this approach for photonic applications has been illustrated by the creation of a suspended defect layer sandwiched between two porous opal films.

METHODS

Fabrication of Colloidal Photonic Crystals. Colloidal SiO_2 and polystyrene spheres with diameters ~300 or 280 nm were synthesized following the emulsion polymerization (30) and Stöber–Fink–Bohn method (31), respectively. The opaline PhCs were then deposited on a 10 × 22 × 0.30 mm^3 glass substrate (microscope glass slides, Marienfeld, Germany) at 55 °C by the convective self-assembly technique (32). Colloids with volume fractions of ~0.1 % were employed.

Deposition of NCs. Commercial CdSe/ZnS-coated Evidots stabilized in water (EviTags, Evident Technologies product) were used as received. The concentration of the nanocolloids was 4.5 nmol/mL, and the average size of the dots was 3.2 nm (the approximate hydrodynamic diameter was 25 nm). The substrate on which the opal had been deposited was preheated on a hot plate at temperatures of 50–105 °C for 5 min. Then, 30 μL of the nanocolloids was drop-coated onto the surface of the opal. The droplet dried within 20 min, leaving behind a ring pattern. The dimensions of the dryout stain pattern could be managed by controlling by the size and concentration of the nanocolloids as well as the evaporation conditions. Before the deposition of a second opal, the sample was annealed at 105 °C for 15 min. Finally, a second opal was grown on top of the NC layer using the same convective self-assembly technique as that described above.

Characterization. The quality of the structure was examined by a field-emission scanning electron microscopy (JEOL JSM-6340F). The reflection measurements were performed using a homemade microscope spectroscopy to determine the optical Bragg diffraction peak from the colloidal crystal planes arising because of the existence of a photonic pseudogap. The light source is focused on the sample on the microscope stage via an objective lens. A miniature fiber-optic spectrometer (Ocean Optics USB2000) was connected to the TV port of a light microscope (Leica, DMLS) via an optical fiber (200 μm diameter) for collecting the reflected/transmitted light.

Acknowledgment. The authors thank Tay Yee Yan from Nanyang Technological University for obtaining the high-resolution TEM images. Support for L.K.T. has been provided through a scholarship awarded by Singapore Millennium Foundation, Singapore.

Supporting Information Available: High-resolution TEM images of the NC film, photoluminescence spectra of the NC solution and NC film, photographs of water and nanocolloid droplets on porous and flat planar substrates, schematic illustration of the evaporation and dry-out process of a nanocolloid droplet on porous and flat planar substrates, and top-view optical microscope images of a typical ring pattern from a dried nanocolloid droplet on a porous substrate. This material is available free of charge via the Internet at http://pubs.acs.org.

REFERENCES AND NOTES

(1) Arsenault, A.; Fleischhaker, F.; von Freymann, G.; Kitaev, V.; Miguez, H.; Mihi, A.; Tétreault, N.; Vekris, E.; Manners, I.; Aitchison, S.; Perovic, D.; Ozin, G. A. *Adv. Mater.* **2006**, *18*, 2779–2785.
(2) Jiang, C. Y.; Markutsya, S.; Pikus, Y.; Tsukruk, V. V. *Nat. Mater.* **2004**, *3*, 721–728.
(3) Baker R. W. *Membrane Technology and Applications*; John Wiley & Sons Ltd.: Chichester, England, 2004.
(4) Striemer, C. C.; Gaborski, T. R.; McGrath, J. L.; Fauchet, P. M. *Nature* **2007**, *445*, 749–753.
(5) Defay, E.; Millon, C.; Malhaire, C.; Barbier, D. *Sens. Actuators A* **2002**, *99*, 64–67.
(6) Davidson, J. L.; Wur, D. R.; Kang, W. P.; Kinser, D. L.; Kerns, D. V. *Diamond Relat. Mater.* **1996**, *5*, 86–92.
(7) Braun, P. V.; Rinne, S. A.; García-Santamaría, F. *Adv. Mater.* **2006**, *18*, 2665–2678.
(8) Wu, Z. C.; Chen, Z. H.; Du, X.; Logan, J. M.; Sippel, J.; Nikolou, M.; Kamaras, K.; Reynolds, J. R.; Tanner, D. B.; Hebard, A. F.; Rinzler, A. G. *Science* **2004**, *305*, 1273–1276.
(9) Goedel, W. A.; Heger, R. *Langmuir* **1998**, *14*, 3470–3474.
(10) Vendamme, R.; Onoue, S. Y.; Nakao, A.; Kunitake, T. *Nat. Mater.* **2006**, *5*, 494–501.
(11) Tétreault, N.; Arsenault, A. C.; Mihi, A.; Wong, S.; Kitaev, V.; Manners, I.; Miguez, H.; Ozin, G. A. *Adv. Mater.* **2005**, *17*, 1912–1916.
(12) Lin, Y.; Skaff, H.; Boker, A.; Dinsmore, A. D.; Emrick, T.; Russell, T. P. *J. Am. Chem. Soc.* **2003**, *125*, 12690–12691.
(13) Huck, W. T. S.; Stroock, A. D.; Whitesides, G. M. *Angew. Chem., Int. Ed.* **2000**, *39*, 1058–1061.
(14) Lim, M. H.; Ast, D. G. *Adv. Mater.* **2001**, *13*, 718–721.
(15) Jin, J.; Wakayama, Y.; Peng, X. S.; Ichinose, I. *Nat. Mater.* **2007**, *6*, 686–691.
(16) Fleischhaker, F.; Arsenault, A. C.; Schmidtke, J.; Zentel, R.; Ozin, G. A. *Chem. Mater.* **2006**, *18*, 5640–5642.
(17) Joannopoulos, J. D. *Photonic crystals: molding the flow of light*; Princeton University Press: Princeton, NJ, 1995.
(18) Reis, N. C., Jr.; Griffiths, R. F.; Santos, J. M. *Appl. Math. Model.* **2008**, *32*, 341–361.
(19) Westin, S. N.; Winter, S.; Karlsson, E.; Hin, A.; Oeseburg, F. *J. Hazard. Mater.* **1998**, *63*, 5–24.
(20) Rogach, A. L.; Talapin, D. V.; Shevchenko, E. V.; Kornowski, A.; Haase, M.; Weller, H. *Adv. Funct. Mater.* **2002**, *12*, 653–664.
(21) Murray, C. B.; Kagan, C. R.; Bawendi, M. G. *Science* **1995**, *270*, 1335–1338.
(22) Tang, Z.; Zhang, Z.; Wang, Y.; Glotzer, S. C.; Kotov, N. A. *Science* **2006**, *314*, 274–278.
(23) Kralchevsky, P. A.; Denkov, N. D. *Curr. Opin. Colloid Interface Sci.* **2001**, *6*, 383–401.
(24) Deegan, R. D.; Bakajin, O.; Dupont, T. F.; Huber, G.; Nagel, S.; Witten, T. *Nature* **1997**, *389*, 827–829.
(25) Koh, Y. K.; Wong, C. C. *Langmuir* **2006**, *22*, 897–900.
(26) Adachi, E.; Dimitrov, A. S.; Nagayama, K. *Langmuir* **1995**, *11*, 1057–1060.
(27) Chon, C. H.; Paik, S.; Tipton, J. B., Jr.; Kihm, K. D. *Langmuir* **2007**, *23*, 2953–2960.
(28) Im, S. H.; Lim, Y. T.; Suh, D. J.; Park, O. O. *Adv. Mater.* **2002**, *14*, 1367–1369.
(29) Jiang, P.; Ostojic, G. N.; Narat, R.; Mittleman, D. M.; Colvin, V. L. *Adv. Mater.* **2001**, *13*, 389–393.
(30) Shim, S.-E.; Cha, Y.-J.; Byun, J.-M.; Choe, S. *J. Appl. Polym. Sci.* **1999**, *71*, 2259–2269.
(31) Stober, W.; Fink, A.; Bohn, E. *J. Colloid Interface Sci.* **1968**, *26*, 62–69.
(32) Jiang, P.; Bertone, J. F.; Hwang, K. S.; Colvin, V. L. *Chem. Mater.* **1999**, *11*, 2132–2140.

AM800188Z